IEEE Open Journal of
Antennas and Propagation

Received 19 August 2022; revised 16 September 2022; accepted 21 September 2022. Date of publication 26 October 2022;
date of current version 7 November 2022.

Digital Object Identifier 10.1109/OJAP.2022.3217067

A Lossy Transmission Line Model for the Scan Impedance of the Infinite Dipole Array

ERIC D. ROBINSON[1,2] (Member, IEEE), AND CAREY M. RAPPAPORT[1] (Fellow, IEEE)

[1]College of Engineering, Northeastern University, Boston, MA 02115, USA

[2]L153, Sensors, Electromagnetics, and EW Department, The MITRE Corporation, Bedford, MA 01730, USA

CORRESPONDING AUTHOR: E. D. ROBINSON (e-mail: robinson.eri@northeastern.edu)

This work was supported by The MITRE Corporation.

ABSTRACT In this paper, an analytical formulation of the infinite dipole array scan impedance is presented. The primary contribution of this work is the introduction of a lossy transmission line analogue which simultaneously models the Floquet modal impedances as well as the reactive properties of the dipole's physical geometry. A scan dependent line inductance is implemented, resulting in accurate impedance predictions at extreme scan angles. The model accurately predicts the input scan impedance of tightly-coupled arrays and connected arrays for a variety of element geometries. Ground planes, substrates, superstrates, and feed structures are also incorporated in the model. Calculated impedances are compared to full-wave electromagnetic models, demonstrating high accuracy predictions from broadside to near 90° in each scan plane. Finally, an array which scans to 60° in each scan plane is rapidly optimized using only the transmission line model and compared to full-wave simulations, achieving a 3:1 VSWR over a 6.1:1 bandwidth, demonstrating the value of the model as a starting point for array design.

INDEX TERMS Dipole arrays, equivalent circuits, tightly coupled dipole array (TCDA), ultra-wideband (UWB) array.

I. INTRODUCTION

DIPOLE arrays are a popular architecture for achieving wideband performance with scan capability, with the additional advantage of improved cross-polarization compared to other wideband elements such as Vivaldi antennas [1]. Notably, the tightly coupled dipole array (TCDA) has been shown in the literature to achieve these features. The TCDA, sometimes called a closely-spaced array, was first proposed by Munk [2] as a practical realization of Wheeler's theoretical infinite current sheet array [3], intended to achieve wide impedance bandwidths using an array of planar dipoles. The "tightly coupled" descriptor refers to the strong capacitive coupling between adjacent elements, which is implemented in order to counteract the inductance caused by a conductive ground plane beneath the dipole elements. Since Munk's initial innovation, a number of TCDA's have been described in the literature, reporting bandwidths including 5:1, 10:1, and 46:1 [4], [5], [6]. Many of these designs incorporate additional design characteristics, including dielectric loading, unique schemes, and frequency selective surfaces, in order to achieve additional bandwidth.

A common technique to begin designing and optimizing such arrays is to leverage an impedance model based on the physical properties of the array. This has been achieved via equivalent circuit models such as Munk's, as well as analytical formulations based on Green's functions by Cavallo et al. [7]. Existing circuit models are lacking however, in that they are often inaccurate at the band edges and at large scan angles in the E-plane, resulting in extensive manual optimization in full-wave electromagnetic solvers. Methods based on Green's functions demonstrate high accuracy but are formulated for 2D current distributions and require approximations for 3D elements, potentially limiting intuition for the relationship between physical parameters and performance.

This work introduces an intuitive representation for the infinite dipole array impedance by modelling the dipole reactances using a lossy transmission line terminated with the

inter-element impedance. Past models [2] have utilized lossless transmission lines for the Floquet modal impedances, but in this paper the Floquet modal transmission lines are used to calculate the series losses on a dipole equivalent transmission line, accurately incorporating both the reactance due to the ground plane and the reactance due to the physical geometry of the element. The result is a versatile model which does not rely on the computation of geometry-dependent Green's functions.

This transmission line model has the advantage of simplicity, with impedance values based on readily calculated physical parameters for common geometries. It is also valid for non-planar designs, such as "egg-crate" PCB configurations and fat wire dipoles. The proposed model is demonstrated to accurately predict the scan impedance for the dipole array, particularly for extreme scan angles. This calculation is possible when the broadside impedance is known a-priori or estimated via the physical element geometry. The model addresses the fundamental scan impedance behavior of the dipoles themselves, regardless of additions such as feed structures, baluns, and frequency selective surfaces (FSS), although it is also capable of incorporating these. Additional array performance properties, such as radiated fields and inter-polarization common-mode behavior, are beyond the scope of most existing circuit models as well as the proposed new model.

Within this paper, Section II summarizes the conventional TCDA circuit model, which is used as a partial basis for the improved model. Section III compares the conventional circuit model and the Green's function approach to full-wave simulations of a wire array, demonstrating their limitations. Section IV describes the new transmission line model and provides formulas for each model parameter. Section V applies the new model to three different dipole array geometries to demonstrate its accuracy and versatility. In Section VI, feed structures are introduced, and the new model is applied to a wide-scanning array optimization problem, showing its value as a starting point for array design. In Section VII, comparisons to other methods and arrays are discussed, as well as future work to expand the scope of the model.

II. THE CONVENTIONAL TCDA EQUIVALENT CIRCUIT MODEL

As a starting point, we will briefly review the existing, conventional model for the TCDA before adapting it to the more general case of a dipole array with arbitrary inter-element impedances. This model for the core scan behavior (not including secondary additions such as baluns or FSS) remains in prominent use in the past 5 years, particularly among leading TCDA research groups [8], [9], [10].

Munk's original TCDA leveraged an equivalent lumped circuit model to represent the scan impedance behavior of the dipole array, and many designs since have likewise relied on equivalent circuits. The most common equivalent circuit is shown in Figure 1. Within the circuit model, the characteristics of the dipole element are described by a series inductance (L_{DIPOLE}) and a coupling capacitance ($C_{COUPLING}$). These components are then connected in series to a set of transmission lines (TL_{SUPER}, TL_{SUB}) in parallel representing the radiation impedance of the embedded element in terms of the forward and back-propagating radiating Floquet modes. The forward propagating mode is modelled as a transmission line connected to a free space modal impedance (Z_0), while the backward propagating mode terminates in a short circuit, representative of the infinite ground plane. The length of the backward-propagation transmission line is set equal to the height of the dipoles above the ground plane (H_{SUB}), while the length of the forward-propagation transmission line is set equal to an optional superstrate thickness (H_{SUPER}).

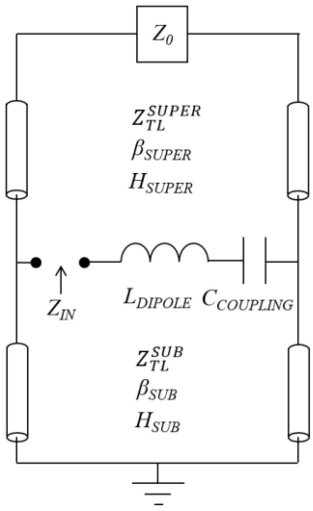

FIGURE 1. The conventional equivalent circuit model for the ideal TCDA input impedance (with ground plane reflector).

The impedance (Z_{SUPER}, Z_{SUB}) and propagation constants (β_{SUPER}, β_{SUB}) of the transmission line segments are determined by the characteristics of the scanned Floquet modes in the media above and below the array, as well as the ratio of the E and H plane element spacing. Munk and others based their formulation of the Floquet scan impedance on that of Wheeler [3], who in turn referenced Stark in his derivation [11]. Wheeler arrived at a scan dependence for the Floquet modes which was equivalent to the field pattern function of the array, $F(\theta)^2$, divided by an aperture foreshortening term $\cos\theta$. It was assumed that $F(\theta)^2$ is equal to $\cos^2\theta$ in the E-plane, with no variation in the H-plane. The result is a Floquet modal impedance that varies according to $\cos\theta$ in the E plane, and $1/\cos\theta$ in the H plane.

The free-space impedance, Z_0, has the same scan and unit cell dependence as the Floquet modes. Unlike the Floquet modal impedance, the propagation constants for the transmission line segments are only geometrically dependent on the component of the propagation vector normal to the array. Thus, a simple $\cos\theta$ term is used to set the propagation

constant of the scanned mode, along with the dielectric properties. Many arrays since Munk's original design, including that of Doane et al. [12], have included a dielectric superstrate to improve the wideband performance of the array. In modelling these arrays, sub-sections of transmission line are introduced with impedance and propagation constants appropriately scaled according to the relative permittivity and permeability of the materials. The impact of refraction on the normal-oriented propagation vector is also accounted for by calculating the angle of refraction θ_R from layer to layer.

Finally, some designs, including Doane's have included models of feed structures which provide a realistic means to supply a signal from beneath the ground plane up to the feed point of the dipole. In the following sections of this paper, we will initially examine the scan impedance without feed structures but will later integrate them into the model for optimization purposes. The full set of equations governing the conventional equivalent circuit model, which align with those reported by Doane, are

$$Z_{TL}^{E} = \frac{d_E}{d_H}\sqrt{\frac{\mu_0\mu_r}{\varepsilon_0\varepsilon_r}}cos\theta_R \tag{1}$$

$$Z_{TL}^{H} = \frac{d_E}{d_H}\sqrt{\frac{\mu_0\mu_r}{\varepsilon_0\varepsilon_r}}\frac{1}{cos\theta_R} \tag{2}$$

$$Z_{0}^{E} = \frac{d_E}{d_H}\sqrt{\frac{\mu_0}{\varepsilon_0}}cos\theta \tag{3}$$

$$Z_{0}^{H} = \frac{d_E}{d_H}\sqrt{\frac{\mu_0}{\varepsilon_0}}\frac{1}{cos\theta} \tag{4}$$

$$\beta_{TL} = \sqrt{\mu_r\varepsilon_r}\ cos\theta_R \tag{5}$$

$$\theta_R = \sin^{-1}\left(\frac{\sin\theta}{\sqrt{\mu_r\varepsilon_r}}\right) \tag{6}$$

where d_E is the array spacing in the E plane, d_H is the array spacing in the H plane, μ_r is the relative permeability of the media, and ε_r is the relative permittivity of the media. Superscripts E and H denote whether the impedance is defined for the E or H plane scan, and the TL and 0 subscripts denote whether the impedance is that of the transmission line sections or upper radiating half-space, respectively.

We note that this conventional circuit model defines the core scan impedance of the array. Various additions such as FSS, multi-layered superstrates, and matching-network integrated feed structures [8], [9], [12] serve primarily to match to this impedance or otherwise modify it. Thus, it is critical to correctly model the core behavior, including both the radiating modes and the reactive properties of the dipole itself, in order to achieve an accurate model.

III. PERFORMANCE OF THE CONVENTIONAL TCDA CIRCUIT MODEL

An accurate model for the scan impedance will minimize error at scan for all scan angles simultaneously. To evaluate the accuracy of the conventional model's scan impedance formulation, a wire TCDA was first simulated with a PEC ground plane and no dielectric superstrate or substrate. The

TABLE 1. Conventional circuit model values of the TCDAs.

	Analytical	Broadside-Fit
Z_{PORT}	100 Ω	100 Ω
$C_{COUPLING}$	0.28 pF	0.33 pF
C_{GAP}	0.56 fF	14.3 fF
L_{DIPOLE}	11.3 nH	11.2 nH
H_{SUB}	2.83 cm	2.83 cm
H_{SUPER}	2.17 cm	2.17 cm
ε_{SUB}	1	1
ε_{SUPER}	1	1
ε_{PCB}	1	1
d_E	1.4 cm	1.4 cm
d_H	2.8 cm	2.8 cm

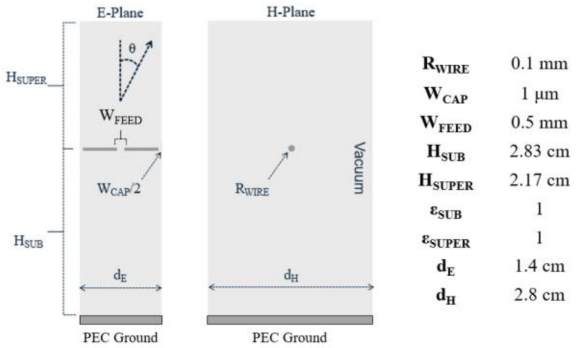

FIGURE 2. Geometry of the simple wire TCDA (not to scale).

inductance and capacitance values for the wire TCDA circuit model were initially estimated analytically based on the dipole dimensions. Afterwards, precise values were numerically optimized by comparing to the full wave model at broadside scan. This allowed for isolating the accuracy of the model's scan dependence from other factors such as specific circuit parameter values.

The analytically estimated and broadside-fit parameters are listed in Table 1 for the example wire TCDA. The input impedance was simulated at broadside as well as at 45° in both the E and H-scan planes. A notional band of 0.5 to 5 GHz was used to demonstrate the wideband accuracy of the lossless equivalent circuit model. The unit-cell geometry of the example TCDA is shown in Figure 2.

The wire TCDA was designed to validate the core scan behavior of the conventional equivalent circuit model; it was not optimized for performance. The capacitive coupling between dipole elements was formed solely by the fields between the tips of adjacent dipoles. To calculate the wire dipole arm inductance, the thin-wire formulation given by Rosa [13] was used

$$L_{DIPOLE} = \frac{\mu}{\pi}\left(l * \log\left(\frac{l+\sqrt{l^2+\rho^2}}{\rho}\right) - \sqrt{l^2+\rho^2} + \frac{l}{4} + \rho\right) \tag{7}$$

where l is the total length of one dipole arm (such that $l = d_E - W_{FEED} - W_{CAP})/2$ and ρ is the radius of the wire, resulting in $L_{DIPOLE} = 11.3$ nH. For the coupling capacitance

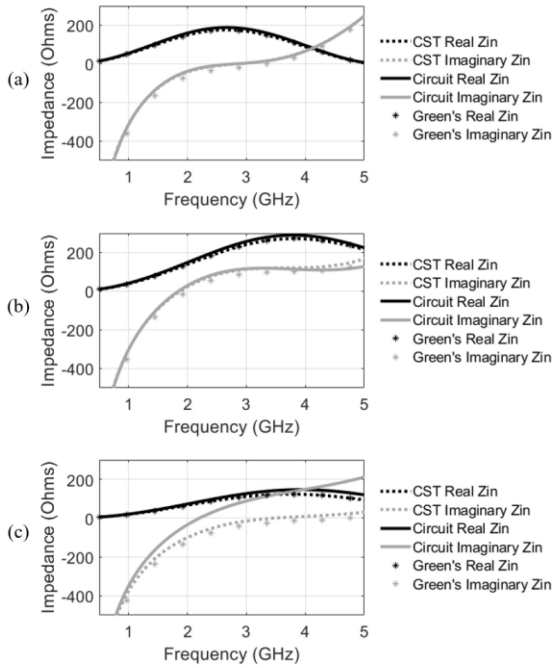

FIGURE 3. (a) Broadside input impedance of the thin wire TCDA, comparison of CST, Conventional Circuit Model, and Green's Function Model (b) H-plane 45 scan with the same parameters, and (c) E-plane 45 scan with the same parameters.

between wire tips, the radius of the wire is approximately 100 times larger than the gap, and thus a parallel plate approximation of the capacitance is sufficient:

$$C_{COUPLING} = \frac{\varepsilon_0 \pi \rho^2}{W_{CAP}} \tag{8}$$

The resulting coupling capacitance is $C_{COUPLING} = 0.28$ pF. In addition to the coupling capacitance, a shunt capacitance C_{GAP} is also included in parallel to the TCDA circuit to account for the capacitance across the dipole feed gap W_{FEED}; this component has been demonstrated in previous models in the literature [14].

Because the analytical calculation of circuit values is only approximate, a minimization algorithm in MATLAB was used to find precise values that generated the least error at broadside. With the exception of the feed gap capacitance (which did not conform to the parallel plate approximation), the error-fit component values were found to be within ∼15% of the analytically calculated values, indicating their physical plausibility. These values were then used in subsequent circuit models in order to ensure that any error was isolated to the scan impedance formulation, and not the individual component values.

Next, the H-plane and E-plane scan impedances were evaluated at 45°, with results shown in Figure 3 compared to full-wave simulations in CST Microwave Studio. While the H-plane scan demonstrates strong agreement on par with that of the broadside impedance, the E-plane scan imaginary impedance for the conventional equivalent circuit is inaccurate, demonstrating excessive series inductance. In Section IV, the cause of this disagreement is explored.

In addition to the conventional circuit model, the predicted impedance using the Green's function model [7] was also plotted in Figure 3. Because the modelled unit cell features a 3D wire and the Green's function approach is 2D, an approximation was used to set the dimensions of the current distribution, wherein the width of the current distribution was equal to four times the radius of the thin-wire [15]. High accuracy was observed for the Green's function method, but the computational implementation was significantly more complex, requiring a double summation of Bessel functions. The Green's function performance was optimized for execution in MATLAB via extensive vectorization and used a bound of $^{+}/_{-}$ 20 samples to approximate the infinite double summation, which achieved convergence. In contrast to the 1600 calculations required for the Green's function method, the conventional circuit model required only two transmission line equations per scan.

IV. THE LOSSY TRANSMISSION LINE MODEL

A. THE TRANSMISSION LINE EQUIVALENT FOR THE SMALL DIPOLE

Several adjustments to the conventional model result in significantly improved accuracy, particularly at large E-plane scan angles. First, it is observed that the conventional circuit model over-simplifies the reactive field behavior of the electrically small dipole comprising the unit cell by omitting the dipole self-capacitance. A more accurate representation may be obtained by considering the dipole as a short, lossy transmission line. This representation is valid due to the field behavior of the radiating structure.

Consider a small subsection of current I_N on one arm of the dipole, shown in Figure 4 (a). The section possesses a series inductance due to the relation of I_N to the surrounding magnetic field flux. The same small section possesses a shunt capacitance due to the arcing electric field lines between the two dipole arms. A radiation resistance is also associated with the small section, corresponding to the energy which couples to the far-field. An equivalent circuit for the lossy small dipole in free space is shown in Figure 4 (b).

This periodic circuit is equivalent to that of a lossy transmission line with zero shunt conductance. Thus, we can model the impedance of the dipole using equations for the lossy transmission line input impedance. Similar models have been previously employed for conical dipole input impedances [16] but have not been applied to infinite arrays. When the small dipole is placed in an infinite array, the radiation resistance is replaced with the Floquet modal impedance based on the lattice spacing, ground plane, superstrate, and substrate. The transmission line is no longer terminated in an open-circuit, but now terminates in the inter-element impedance, as shown in Figure 5. Practically, the distributed properties of the transmission line can be approximated by taking the total inductance and capacitance associated with

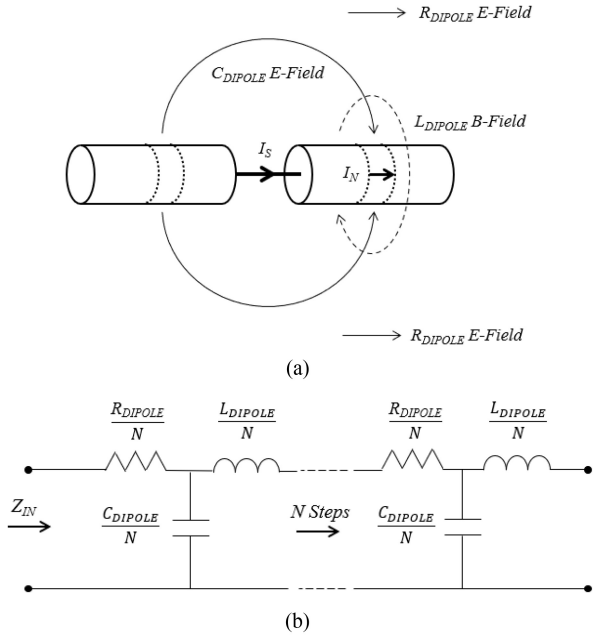

FIGURE 4. (a) Field behavior of an electrically short dipole of constant current and (b) the periodic lumped element transmission line equivalent of the same.

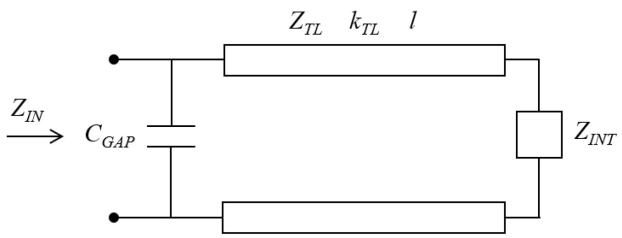

FIGURE 5. The lossy transmission line circuit model for the infinite dipole array input impedance.

the small dipole and dividing it by the length of the line for use in the transmission line equation.

B. THE DIPOLE INDUCTANCE SCAN FACTOR

When simulating the E-45° scan impedance for the ideal wire TCDA (Figure 3), it is evident that the imaginary impedance is overestimated by the conventional model in Section III; this directly corresponds to an excess of series inductance in the circuit. Both Wheeler [3] and Stark [11] expressed the variation of dipole radiation resistance in terms of the field pattern function $F_m(\theta)^2$ divided by a $cos\theta$ factor due to the foreshortening of the projected radiating aperture with scan. For a simulation utilizing impressed voltage sources, the currents on the array vary with scan according to the pattern function. As the currents determine both the resistance and reactance of the impedance, it is evident that any component of the reactance which experiences the same currents as the resistance will also vary with scan according to the same dependence.

Within the lossy transmission line model, the line inductance is in series with the radiation resistance and thus also varies according to the pattern function. Unlike the resistance, however, the scan reactance does not have an aperture dependence since the corresponding energy is not radiated; thus, no $cos\theta$ factor is divided out. Consequently, the inductance can be understood to vary from its broadside value according to the normalized $F_m(\theta)^2$ as the array scans. For a short dipole length ($l < \lambda/4$), the dipole inductance $L_{DIPOLE}(\theta)$ for the transmission line model of the dipole array effectively varies according to

$$H - Scan: L_{DIPOLE}(\theta) = L_B \tag{9}$$

$$E - Scan: L_{DIPOLE}(\theta) = L_B|cos(\theta)|^2 \tag{10}$$

where L_B denotes the inductance at broadside, which can be estimated with (7). The validity of the inductance scan dependence is demonstrated in Section V for all elevation angles when scanning in the E-plane.

C. LOSSY TRANSMISSION LINE MODEL VALUES

Incorporating the aforementioned effects, the generalized lossy transmission line model is shown in Figure 5. The transmission line is terminated in the inter-element impedance Z_{INT}, and a shunt capacitance C_{GAP} is included at the feed ports to account for the capacitance across the dipole feed gap. In the case of the TCDA, Z_{INT} is equal to the impedance of the capacitance between dipoles, $C_{COUPLING}$. For a connected dipole array, $Z_{INT} = 0$.

The transmission line input impedance is given according to the shunt combination of the feed gap capacitance with the classic transmission line input impedance:

$$Z_{IN} = \frac{1}{j\omega C_{GAP}} || Z_{TL} \frac{Z_{INT} + jZ_{TL}tan(k_{TL}l)}{Z_{TL} + jZ_{INT}tan(k_{TL}l)} \tag{11}$$

where Z_{TL} is the characteristic impedance of the lossy transmission line analogue, k_{TL} is the complex propagation constant of the line, and l is the length of the line, equal to half the length of the dipole. These values are calculated using the lossy transmission line equations with the shunt conductance set equal to zero:

$$Z_{TL} = \sqrt{\frac{Z_{RAD}(\theta) + j\omega L_{DIPOLE}(\theta)}{j\omega C_{DIPOLE}}} \tag{12}$$

$$k_{TL} = (1/l)\sqrt{-(Z_{RAD}(\theta) + j\omega L_{DIPOLE}(\theta))(j\omega C_{DIPOLE})} \tag{13}$$

In (12) and (13) C_{DIPOLE} is the self-capacitance of the dipole, $L_{DIPOLE}(\theta)$ is the scan-dependent self-inductance of the dipole, and $Z_{RAD}(\theta)$ is the scan-dependent radiation impedance. Note the $(1/l)$ term in (13) corresponds to the conversion from total dipole parameter values to per-unit-length values such that the propagation constant k_{TL} is appropriately scaled. The term $Z_{RAD}(\theta)$ is the parallel combination of the backward and forward propagating Floquet modal impedances, calculated according to:

$$Z_{RAD}(\theta) = Z_{IN}^{SUB} || Z_{IN}^{SUPER} \tag{14}$$

TABLE 2. TL model values of the wire TCDA.

	Analytical	Broadside-Fit
$C_{COUPLING}$	0.28 pF	0.29 pF
C_{DIPOLE}	44.5 fF	59.1 fF
C_{GAP}	0.56 fF	3.3 fF
L_{DIPOLE}	11.3 nH	11.6 nH

In (14), Z_{IN}^{SUB} and Z_{IN}^{SUPER} are the scan-dependent input impedances of the superstrate and substrate Floquet transmission line analogues shown in Fig. 1, whose parameters are described in (1) - (6). The value of $Z_{RAD}(\theta)$ serves the role of series resistance per unit-length in a conventional lossy transmission line equation. For this model, a complex impedance is necessary to represent this value due the potential inclusion of a ground plane, superstrates, and substrates which contribute a reactive component. This reactance corresponds to the reflection of radiated field components due to these additions. In contrast, $L_{DIPOLE}(\theta)$ and C_{DIPOLE} correspond to the reactive behavior associated with the physical geometry of the element itself.

The self-capacitance C_{DIPOLE} must now be incorporated, and it is useful to have an analytical approximation. A simple approximation for the self-capacitance has been provided by McDonald [17]:

$$C_{DIPOLE} \approx \frac{\pi \varepsilon l}{2\ ln\left(\frac{l}{2\rho}\right)} \tag{15}$$

where l is the length of one dipole arm ($l = d_E/2 = 0.7$ cm), and ρ is the radius of the wire ($\rho = R_{WIRE} = 0.1$ mm). This approximation holds true for short dipoles with small feed gaps and uniform current. The resulting self-capacitance for the wire TCDA example is found to be $C_{DIPOLE} = 44.5$ fF; upon performing a broadside error-fit, a physically plausible value of $C_{DIPOLE} = 59.1$ fF was found to be ideal. In Table 2, the analytically calculated values for the wire TCDA are listed, as well as new error-fit values at broadside for the improved model. For most parameters, the error-fit values for the new model are closer to the analytically-calculated values than the original model values shown in Section II.

V. VALIDATION OF TRANSMISSION LINE MODEL WITH FULL-WAVE SOLVER

A. THE TRANSMISSION LINE EQUIVALENT FOR THE SMALL DIPOLE

Using the lossy transmission line model with the error-fit values in Table 3, the scan impedance is calculated and compared to the impedance from a CST full-wave model in Figure 6, demonstrating near-perfect agreement for 45° scan. Furthermore, the scan impedance is also plotted for 60° and 85° in the E and H-planes, showing equally good agreement. There is no change in the broadside impedance observed in Figure 3. With the model now proven to accurately represent the scan impedance behavior for a thin wire TCDA, it is next applied to other dipole array geometries.

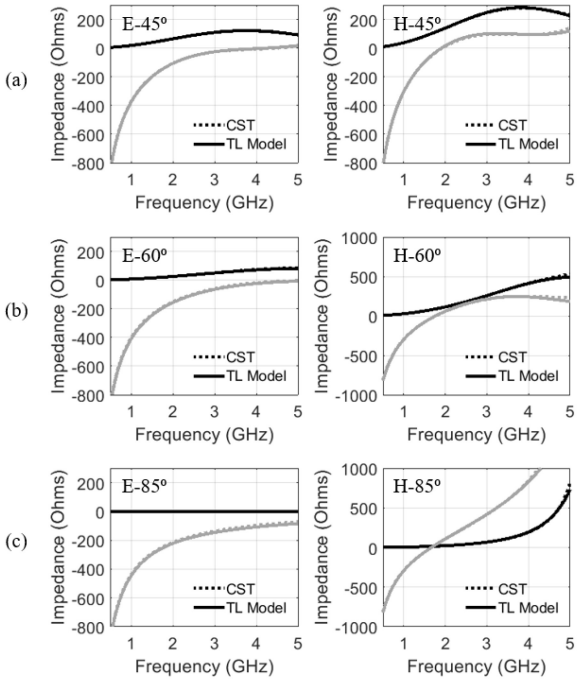

FIGURE 6. (a) E and H plane 45° real (black) and imaginary (grey) scan input impedance of the thin wire TCDA, comparison of CST and Transmission Line Model, (b) E and H plane 60° scan (c) E and H plane 85° scan.

TABLE 3. TL model values of the fat wire connected array.

	Analytical	Broadside-Fit
Z_{INT}	0	0
C_{DIPOLE}	0.10 pF	0.14 pF
C_{GAP}	55.6 fF	84 fF
L_{DIPOLE}	5.38 nH	4.63 nH

B. THE FAT WIRE CONNECTED DIPOLE ARRAY

To demonstrate the robustness of the transmission line model, it is next applied to a fat-wire ($\rho > l/10$), connected dipole array with a PEC ground plane. All geometric parameters shown in Figure 2 are preserved except for R_{WIRE}, which was set equal to 0.1 cm (a 10x increase), and W_{CAP} which was set equal to 0. Analytical estimates for each model parameter, as well as the minimized-error broadside fit, are given in Table 3, showing strong physical plausibility. The modelled impedance is plotted in Figure 7, again demonstrating near-perfect agreement with the full-wave model. Note that while the 85° scan was not plotted here for sake of brevity, it had similar near-perfect agreement.

C. THE PCB TIGHTLY-COUPLED DIPOLE ARRAY

To further validate the transmission line model, it was also applied to the PCB TCDA described by Doane, with an ideal feed port [12]. All geometric parameters were duplicated, and the plotted results were re-created to ensure a direct comparison (not shown for brevity). This model represents a significantly more complex geometry, including a tapered dipole feed section, overlapping capacitive sections, and dielectric superstrate. As was done previously for the wire TCDA, values were fit to the model at broadside,

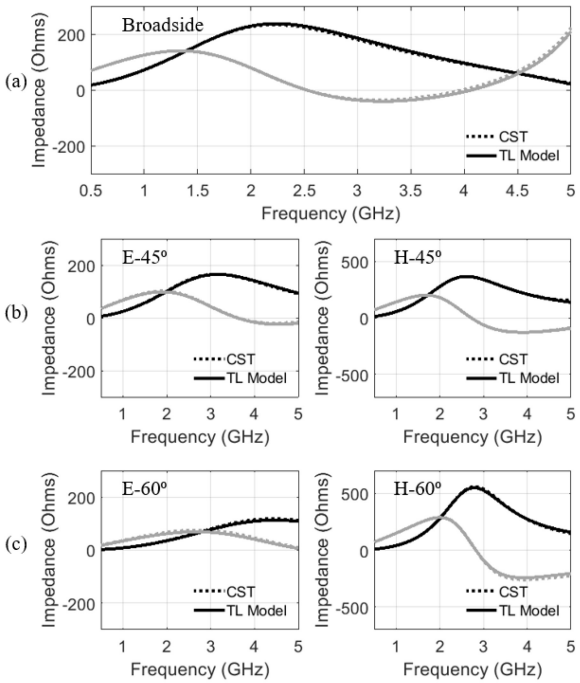

FIGURE 7. (a) Broadside real (black) and imaginary (grey) input impedance of the fat wire connected dipole array, comparison of CST and Transmission Line Model (b) E and H plane 45° scan (c) E and H plane 60° scan.

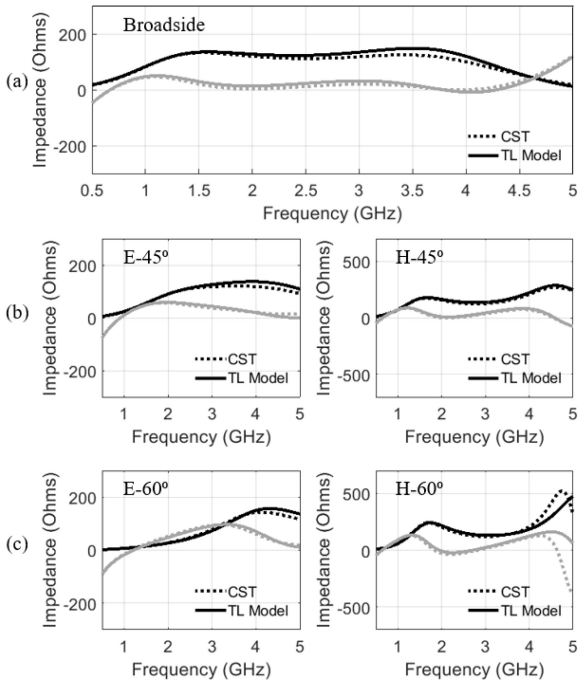

FIGURE 8. (a) E and H plane 45° real (black) and imaginary (grey) scan input impedance of the PCB TCDA, comparison of CST and Transmission Line Model, (b) E and H plane 45° scan (c) E and H plane 60° scan.

TABLE 4. TL model values of the PCB TCDA.

	Originally Calculated	Broadside-Fit
$C_{COUPLING}$	2 pF	2.7 pF
C_{DIPOLE}	N/A	65 fF
C_{GAP}	N/A	79 fF
L_{DIPOLE}	3 nH	4.2 nH

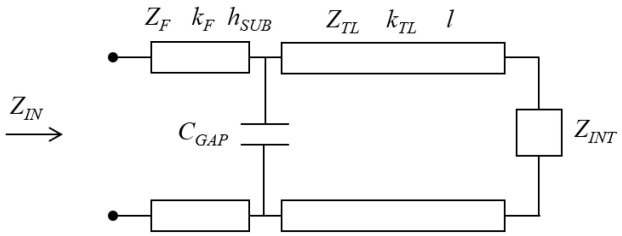

FIGURE 9. The lossy transmission line circuit model for the infinite dipole array input impedance with vertical balanced feed structures.

and then used when calculating the scan impedance. The original values used by Doane, as well as the broadside error-fit values, are shown in Table 4; the error-fit values are physically plausible given the dimensions of the dipole arms. The lossy transmission line impedance model at broadside scan is shown in Figure 8 (a); the E and H-plane scan impedances at 45° and 60° are shown in (b) and (c), demonstrating close agreement over the band. Although not shown for sake of brevity, the transmission line model better predicts the impedance compared to [12].

Note that the agreement between the circuit model and the full-wave simulation is degraded at the upper edge of the band for the 60° H-plane scan. This is because the PCB TCDA features a tapered feed, which results in a variation in the element reactance. In a future effort, this effect could be incorporated by cascading multiple sections of lossy transmission line with varying reactive properties instead of a single line.

VI. OPTIMIZATION OF A WIDE-SCANNING DIPOLE ARRAY WITH FEED STRUCTURES

A. DESIGN GOALS AND OPTIMIZATION MODEL

To demonstrate the value of the transmission line model for practical array designs, a notional wide-scanning array was designed using the model. A single-polarized TCDA was optimized in MATLAB using the methodology described in Section IV to scan out to 60° in both the E and H planes while maximizing the 3:1 VSWR bandwidth. The design was then validated in CST for each scan angle. Feed structures were included in the form of two vertical conductors which form a balanced twin-lead transmission line from the ground plane to the dipole feed point. The purpose of this optimization was not to demonstrate a final, immediately realizable design, but to show the accuracy of the transmission line model for a challenging problem that is beyond the capability of existing circuit models.

In order to incorporate the balanced vertical feed structure, the model was adjusted to add a lossless input transmission line, shown in Figure 9. The feed line parameters are given by its characteristic impedance, propagation constant, and the height of the dipole array above the ground plane, given by Z_F, k_F, and H_{SUB}, respectively. For purposes of the optimizing the array, Z_F and k_F can be approximated using equations

for the twin-lead line capacitance and inductance [18]:

$$C_F = \frac{\varepsilon_{rsub}\varepsilon_0\pi}{\cosh^{-1}\left(\frac{S_F}{D_F}\right)} \tag{16}$$

$$L_F = \frac{\mu_0}{\pi}\cosh^{-1}\left(\frac{S_F}{D_F}\right) \tag{17}$$

$$Z_F = \sqrt{L_F/C_F} \tag{18}$$

$$k_F = \omega\sqrt{L_F C_F} \tag{19}$$

where S_F is the center-to-center spacing between the twin lead conductors, and D_F is the diameter of each conductor. The dipole arms extend to the edges of twin lead conductors, such that the feed gap $W_{FEED} = S_F - D_F$. The substrate dielectric is included between the vertical feed structures.

Due to the presence of the vertical conductors of the feed line, the backward propagating Floquet modal impedance changes; it is no longer scan dependent in the E scan plane due to the shorting of vertically polarized electric fields beneath the array [10]. Likewise, the propagation constant is no longer scan dependent:

$$Z^E_{TLSUB} = \frac{d_E}{d_H}\sqrt{\frac{\mu_0\mu_r}{\varepsilon_0\varepsilon_{rsub}}} \tag{20}$$

$$\beta_{TLSUB} = \sqrt{\mu_r\varepsilon_{rsub}} \tag{21}$$

B. ARRAY GENETIC OPTIMIZATION SETUP

In order to optimize the full-wave design, a genetic algorithm was implemented in MATLAB, adapted from Gordy [19]. The genome for the algorithm consisted of the geometric dimensions of each aspect of the array, along with the superstrate and substrate dielectric properties. The Floquet transmission line model parameters were calculated based on these dimensions using the equations previously listed in (1)-(8). These formulations are generally accurate, with the exception of the approximations for the dipole self-capacitance and self-inductance which feature more variance. To circumvent this limitation, a dipole wire radius W_{RAD} of 0.1 cm was used and held static. Based on the previous section simulating the fat dipole connected array with this same radius, the per-unit length capacitance and inductance can be calculated as 0.1 pF/meter, and 330 nH/meter, respectively. Thus, for the genetic optimization, the broadside self-capacitance and self-inductance are determined only by changes in d_E and the superstrate permittivity, which linearly scales the self-capacitance.

Fitness for the algorithm was defined as the ratio of the maximum to minimum frequency values within the largest span having 3:1 or better VSWR. A frequency band of 0.1 to 5 GHz was simulated to allow for optimal fitness within a subset of a large potential bandwidth of operation. A 100 Ω feed port impedance was specified when calculating VSWR for the array.

C. TCDA OPTIMIZATION RESULTS AND CST COMPARISON

The genetic algorithm for the TCDA optimization converged to a maximum fitness after simulating 310 generations of 100 candidates using the transmission line model at both scan angles as well as broadside, totaling 93,000 simulations. The total duration of the optimization was approximately 60 seconds using an 11th Gen Intel Core i7-1185G7 consumer-grade CPU. The optimal genome is listed in Table 5, with a tightly-coupled array resulting. The modelled optimized bandwidth ranged from 0.41 GHz to 2.6 GHz, resulting in a predicted bandwidth of ~6.3:1.

Using these parameters, along with the predetermined wire radius, the unit cell was then generated and simulated in CST. The resulting unit cell geometry is shown in Figure 10, with a zoomed in view at the connection point between the dipole arms and the vertical feed structures. The array geometry

TABLE 5. Optimized wide-scanning TCDA genome.

Parameter	Optimized Value
R_{WIRE}	0.1 cm
W_{FEED}	0.93 mm
dE	1.94 cm
dH	2.47 cm
H_{SUB}	5.09 cm
H_{SUPER}	2.38 cm
ε_{SUPER}	2.5
ε_{SUB}	1.0
D_F	0.78 mm
S_F	2.33 mm
C_{GAP}	14 µm

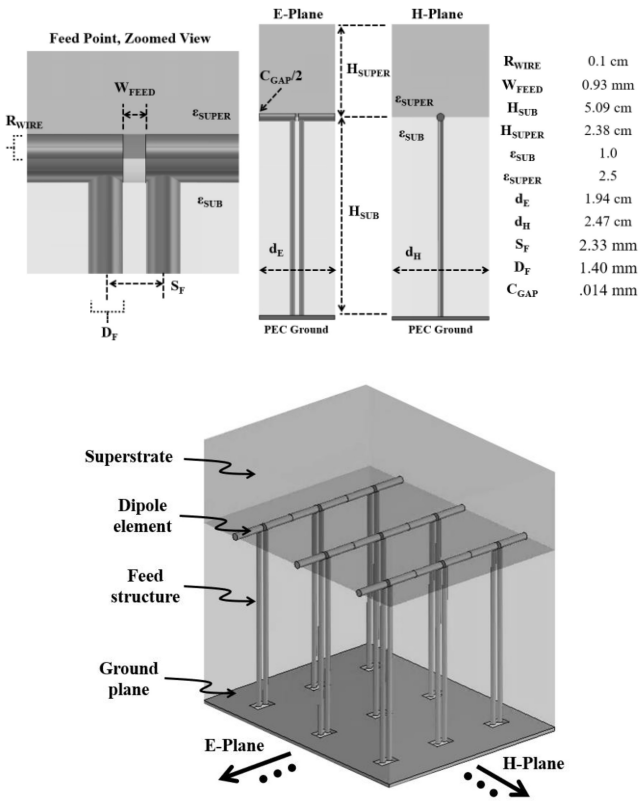

FIGURE 10. Geometry of the optimized dipole array unit cell, with zoomed in Feed Point View (top), and 3D view of multiple unit cells in the infinite array configuration (bottom).

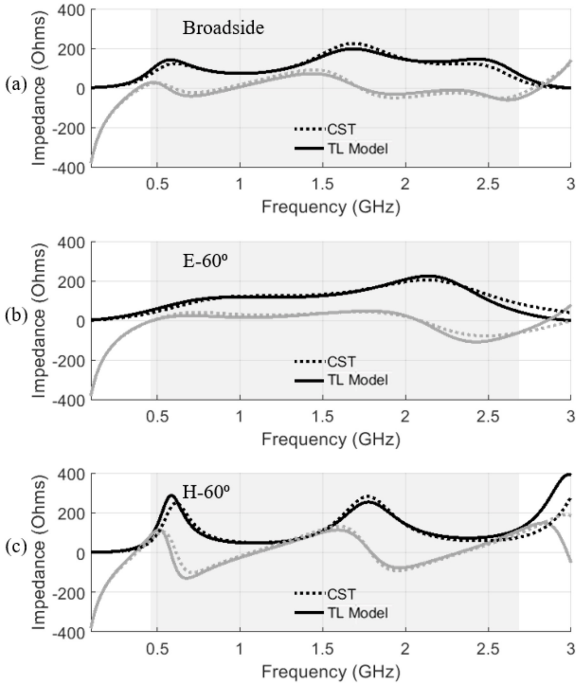

FIGURE 11. (a) Broadside real (black) and imaginary (grey) input impedance of the optimized array, comparison of CST and Transmission Line Model, (b) E plane 60° scan (c) H plane 60° scan.

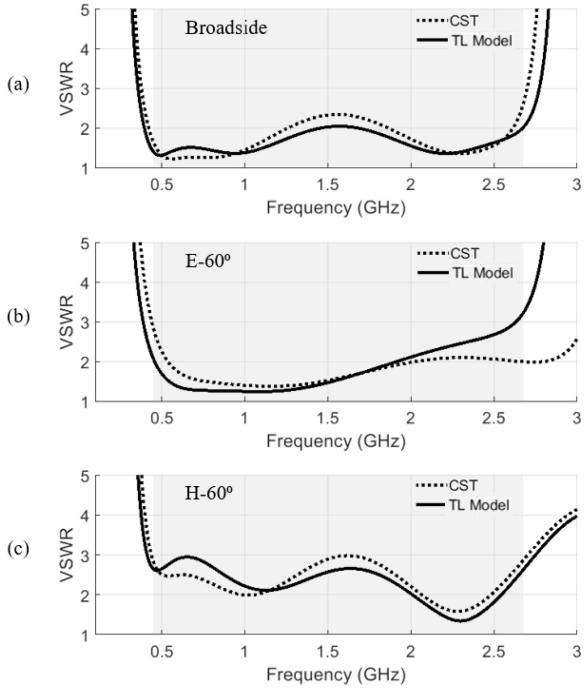

FIGURE 12. (a) Broadside VSWR of the optimized array, comparison of CST and Transmission Line Model, (b) E plane 60° VSWR (c) H plane 60° VSWR.

is realizable for fabrication with the possible exception of the capacitive gaps between dipole arms. The interelement capacitance was modelled in CST with a parallel plate geometry, which required a very small gap (14 μm) to achieve the optimized capacitance. In an actual array, an alternative capacitive structure may be needed due to fabrication tolerances, such as interdigitated fingers at the ends of the dipole arms or larger diameter capacitive plates.

A comparison of the simulated scan impedance between the lossy transmission line model and the full-wave CST model is plotted in Figure 11. No broadside fit or other optimization of parameter values was utilized for this comparison. Strong agreement is observed for each scan angle over a greater than 10:1 simulated bandwidth, especially in the matched band (shaded gray region). The only area demonstrating disagreement occurs at ∼3.0 GHz in the H-plane scan, possibly due to the presence of the vertical feed transmission lines affecting the dipole self-reactance, causing the parameter estimates to be less accurate.

The VSWR of the full-wave design is shown in Figure 12, demonstrating good agreement across the matched band. The full-wave design based on the transmission line model exhibits less than 3:1 VSWR from 0.44 – 2.7 GHz, resulting in a 6.1:1 bandwidth. While a very slight deviation has occurred from the MATLAB transmission line model matched bandwidth, these differences may be corrected by limited full-wave optimization and tweaking. The total thickness of the array is equal to ∼0.11 λ at 0.44 GHz.

VII. DISCUSSION AND CONCLUSION

In this paper, a new model was described which leverages lossy transmission line equations to accurately predict the scan impedance of the infinite dipole array. The model demonstrates high accuracy when the broadside array impedance is known a-priori or estimated via physical parameters. It correctly predicts the scan impedance at much greater angles than previously reported lumped element circuit models, particularly in the E-scan plane. It also enables accurate predictions for geometries that are not readily described by existing Green's function based models for 2D current distributions, such as Doane's PCB TCDA.

The model was shown to be valid for tightly-coupled arrays and connected dipole arrays with a variety of geometries (thin wire, fat wire, and PCB). Although not explored here, arbitrary interelement impedances via lumped components are likewise possible, as well as arrays without ground planes and asymmetric dipole elements. The model is compatible with potential inclusions of popular TCDA design additions, such as FSS, matching network feed structures, and multi-layered superstrates.

The value of the model was demonstrated by using it to optimize a notional array to maximize bandwidth at large scan angles in both the E and H planes. Optimizing the transmission line model via genetic algorithm (with some parameters known a-priori) required roughly 60 seconds with an affordable consumer-grade processor. Near perfect agreement was observed between the model and the full-wave simulation over the matched band.

The optimized array design features a fractional bandwidth of 146%, which greatly exceeds the bandwidth of the individual dipole element in free-space; this is enabled by the careful optimization of parameters such as inter-element capacitance. Although the optimized design is largely notional and is intended primarily to demonstrate the accuracy of the transmission line model when used for optimization, we note that the performance is comparable to other published designs such as [20], which featured a 3.1:1 VSWR with at least 60° scan in each plane and achieved a bandwidth of 6.1:1.

In practice, parameters other than bandwidth are also of interest in the design of the unit cell, such as cross-polarization isolation and efficiency. While the transmission line impedance model does not predict these behaviors, it offers a robust starting point for the design of a wide-scanning array, particularly when some parameters such as unit cell size or conductor dimensions are predetermined. Because the model is based on reactive parameters directly related to the element physical dimensions, it also offers an intuitive understanding of performance for post-optimization tweaking in full-wave design software.

We note that one limitation of the current lossy transmission line model is its dependency on the reactive approximation for a short dipole; this enables the use of fixed reactive values along the length of the dipole equivalent transmission line. For increasing dipole lengths ($d_E \rightarrow \lambda/2$), however, these values will not be fixed due to the field behavior of the dipole varying across its length. One workaround for this issue to design a short dipole ($d_E = \lambda/4$) but choose an array lattice spacing that spatially oversamples in the E-scan plane, and then feed adjacent element rows in parallel for an effective half-wavelength phase-center spacing. This approach has been successfully demonstrated by Doane et al. [12].

The next task in this work will be to fabricate and test a dipole array designed using the lossy transmission line model; doing so will further compare to the model and demonstrate its value. Subsequent efforts may investigate improving accuracy for long dipole elements based on varying reactive parameters along the lossy transmission line. Additionally, the model may be adapted to tapered dipole slot hybrids such as [21] by implementing a cascade of transmission line sections with similarly varying parameters. Unbalanced feed structures may also be investigated by implementing appropriate reactive loading on the input transmission line. Higher order matching techniques and incorporation of matching baluns may also be incorporated to further expand the bandwidth of rapidly optimized wide-scanning arrays. Finite array effects are also a topic of significant interest and will be explored in the context of the new model, potentially by incorporating additional line segments to represent the effects of surface wave modes.

ACKNOWLEDGMENT

The authors would like to thank Dr. Steve Best, Dr. Wajih Elsallal, Dr. Ian McMichael, and Dr. Chris Niessen of The MITRE Corporation for their input and support in the course of this research.

REFERENCES

[1] D. McGrath, N. Schuneman, T. Shively, and J. Irion, "Polarization property of scanning slot phased array," in *Proc. IEEE Int. Symp. Phased Array Syst. Technol.*, Jan. 2004, pp. 295–299.
[2] B. A. Munk, *Finite Antenna Arrays and FSS*. Piscataway, NJ, USA: Wiley-Intersci., 2003.
[3] H. A. Wheeler, "Simple relations derived from a phased-array antenna made of an infinite current sheet," *IEEE Trans. Antennas Propag.*, vol. 13, no. 4, pp. 506–514, Jul. 1965.
[4] S. S. Holland and M. N. Vouvakis, "The planar ultrawideband modular antenna (PUMA) array," *IEEE Trans. Antennas Propag.*, vol. 60, no. 1, pp. 130–140, Jan. 2012, doi: 10.1109/TAP.2011.2167916.
[5] M. W. Elsallal and J. C. Mather, "An ultra-thin, decade (10:1) Bandwidth, modular 'BAVA' array with low cross-polarization," in *Proc. IEEE Int. Symp. Antennas Propag. (APSURSI)*, Spokane, WA, USA, 2011, pp. 1980–1983, doi: 10.1109/APS.2011.5996893.
[6] A. D. Johnson, J. Zhong, S. B. Venkatakrishnan, E. A. Alwan, and J. L. Volakis, "Phased array with low angle scanning and 46:1 bandwidth," *IEEE Trans. Antennas Propag.*, vol. 68, no. 12, pp. 7833–7841, Dec. 2020, doi: 10.1109/TAP.2020.2998869.
[7] D. Cavallo, A. Neto, and G. Gerini, "Analytical description and design of printed dipole arrays for wideband wide-scan applications," *IEEE Trans. Antennas Propag.*, vol. 60, no. 12, pp. 6027–6031, Dec. 2012, doi: 10.1109/TAP.2012.2209856.
[8] A. D. Johnson, "Ultra-wideband phased arrays for small mobile platforms," Ph.D. dissertation, Dept. Electr. Comput. Eng., Florida Int. Univ., Miami, FL, USA, 2019. [Online]. Available: https://digitalcommons.fiu.edu/etd/4222
[9] M. H. Novak, F. A. Miranda, and J. L. Volakis, "Ultra-wideband phased array for millimeter-wave ISM and 5G bands, realized in PCB," *IEEE Trans. Antennas Propag.*, vol. 66, no. 12, pp. 6930–6938, Dec. 2018, doi: 10.1109/TAP.2018.2872177.
[10] S. Kim and S. Nam, "A novel reflection-type polarization convertor design using connected orthogonal tightly coupled dipole arrays," *IEEE Access*, vol. 10, pp. 52116–52125, 2022, doi: 10.1109/ACCESS.2022.3175161.
[11] L. Stark, "Radiation resistance of a dipole in an infinite array," *Radio Sci.*, vol. 1, no. 3, pp. 361–377, Mar. 1966.
[12] J. P. Doane, K. Sertel, and J. L. Volakis, "A wideband, wide scanning tightly coupled dipole array with integrated balun (TCDA-IB)," *IEEE Trans. Antennas Propag.*, vol. 61, no. 9, pp. 4538–4548, Sep. 2013, doi: 10.1109/TAP.2013.2267199.
[13] E. B. Rosa, "The self and mutual inductances of linear conductors," *Bull. Bureau Stand.*, vol. 4, no. 2, pp. 301–344, 1908.
[14] E. A. Alwan, K. Sertel, and J. L. Volakis, "Circuit model based optimization of ultra-wideband arrays," in *Proc. IEEE Int. Symp. Antennas Propag.*, 2012, pp. 1–2, doi: 10.1109/APS.2012.6348919.
[15] S. Tretyakov, *Analytical Modelling in Applied Electromagnetics*. Norwood, MA, USA: Artech House, Inc., 2003.
[16] S. A. Schelkunoff, "Theory of antennas of arbitrary size and shape," in *Proc. IRE*, vol. 29, no. 9, pp. 493–521, Sep. 1941, doi: 10.1109/JRPROC.1941.231669.
[17] K. T. McDonald, *Reactance of Small Antennas*. Princeton, NJ, USA: Princeton Univ., Sep. 2011.
[18] D. Pozar, *Microwave Engineering*. New York, NY, USA: Wiley, 2005.
[19] M. B. Gordy, "GA.M: A MATLAB routine for function maximization using a genetic algorithm," *J. Bus. Econ. Statist.*, vol. 13, no. 1, Jan. 1995.
[20] E. Yetisir, N. Ghalichechian, and J. L. Volakis, "Ultrawideband array with 70° scanning using FSS superstrate," *IEEE Trans. Antennas Propag.*, vol. 64, no. 10, pp. 4256–4265, Oct. 2016, doi: 10.1109/TAP.2016.2594817.
[21] R. W. Kindt and M. W. Elsallal, "Low-profile machined-metal array radiator for Ka-Band," in *Proc. IEEE Int. Symp. Antennas Propag. North Amer. Radio Sci. Meeting*, 2020, pp. 287–288, doi: 10.1109/IEEECONF35879.2020.9330075.

ERIC D. ROBINSON (Member, IEEE) received the B.S. and M.S. degrees in electrical engineering from the Georgia Institute of Technology, Atlanta, GA, USA, in 2014 and 2015, respectively. He is currently pursuing the Ph.D. degree in electrical engineering with Northeastern University, Boston, MA, USA. In 2016, he was hired by The MITRE Corporation, Bedford, MA, USA, as an Antennas and Electromagnetics Engineer, and in 2021, he was promoted to a Lead Engineer. His current research interests include ultrawideband phased arrays, additively manufactured arrays, vector sensing arrays, and radio direction finding methods.

CAREY M. RAPPAPORT (Fellow, IEEE) received the S.B. degree in mathematics and the S.B., S.M., and E.E. degrees in electrical engineering from the Massachusetts Institute of Technology (MIT), Cambridge, MA, USA, in 1982, and the Ph.D. degree in electrical engineering from MIT in June 1987. He joined the Electrical and Computer Engineering Faculty, Northeastern University, Boston, MA, USA, in 1987. In 1995, he was a Fulbright Scholar Visiting Professor with the Electromagnetics Institute, Technical University of Denmark, Lyngby, Denmark. In 2005, he was a Visiting Research Scientist with CSIRO, Epping, NSW, Australia. He has consulted for CACI, Alion Science and Technology, Inc., Geo-Centers, Inc., PPG, Inc., and several municipalities on wave propagation and modeling, and microwave heating and safety. He was a Principal Investigator (PI) of an ARO-sponsored Multi-Disciplinary University Research Initiative in Humanitarian Demining and a Co-PI of the NSF-sponsored CenSSIS Engineering Research Center and the U.S. Department of Homeland Security Awareness and Localization of Explosives-Related Threats Center of Excellence. In 2011, he was appointed as a College of Engineering Distinguished Professor. He has authored over 430 technical journal and conference papers in the areas of microwave antenna design, electromagnetic wave propagation and scattering computation, and bioelectromagnetics. He holds two reflector antenna patents, two biomedical device patents, and four subsurface sensing device patents. He is a member of Sigma Xi and Eta Kappa Nu professional honorary societies.